Cell, Vol. 120, 599–611, March 11, 2005, Copyright ©2005 by Elsevier Inc. DOI 10.1016/j.cell.2004.12.037

A Unique RNA Fold in the RumA-RNA-Cofactor Ternary Complex Contributes to Substrate Selectivity and Enzymatic Function

Tom T. Lee,[1,2] Sanjay Agarwalla,[1,2] and Robert M. Stroud[1,*]
[1]Department of Biochemistry and Biophysics
University of California, San Francisco
San Francisco, California 94143

Summary

A single base (U1939) within *E. coli* 23S ribosomal RNA is methylated by its dedicated enzyme, RumA. The structure of RumA/RNA/*S*-adenosylhomocysteine uncovers the mechanism for achieving unique selectivity. The single-stranded substrate is "refolded" on the enzyme into a compact conformation with six key intra-RNA interactions. The RNA substrate contributes directly to catalysis. In addition to the target base, a second base is "flipped out" from the core loop to stack against the adenine of the cofactor *S*-adenosylhomocysteine. Nucleotides in permuted sequence order are stacked into the site vacated by the everted target U1939 and compensate for the energetic penalty of base eversion. The 3′ hairpin segment of the RNA binds distal to the active site and provides binding energy that contributes to enhanced catalytic efficiency. Active collaboration of RNA in catalysis leads us to conclude that RumA and its substrate RNA may reflect features from the earliest RNA-protein era.

Introduction

Posttranscriptional modifications of nucleotides in RNA are present in all kingdoms of life. These occur in many types of RNAs, including tRNA, rRNA, mRNA, snRNA, snoRNA, and tmRNA. A total of 96 distinct types of modified nucleotides in RNA have been identified so far (Rozenski et al., 1999) (http://medstat.med.utah.edu/RNAmods). Certain modifications, such as methylation, pseudouridylation, and thiouridylation, occurred early in the evolution of life (Anantharaman et al., 2002), and a role for modified nucleotides in the transition from the RNA world to the present DNA-protein world has been suggested (Martinez Gimenez et al., 1998). Almost all 35 modifications found in the *E. coli* ribosome are clustered at functionally important sites, particularly the peptidyltransferase center; the A, P, and E sites of tRNA binding sites; the mRNA binding site; the polypeptide exit tunnel; and the subunit interface (Decatur and Fournier, 2002). Although none of these modifications has been found to be absolutely essential for ribosomal function, they are believed to improve ribosomal efficiency on a global level (Decatur and Fournier, 2002).

A common modification found in RNA is the substitution of 5-methyluridine (m^5U) for uridine. This modification is catalyzed by *S*-adenosylmethionine (SAM)-dependent m^5U methyltransferases (MTases) that are position specific. RumA specifically catalyzes the formation of m^5U at 1939 in 23S rRNA of *E. coli* (Agarwalla et al., 2002). In addition to rumA, *E. coli* contains two additional m^5U MTase genes, trmA and rumB, that are responsible for the formation of tRNA m^5U54 (Kealey et al., 1994) and 23S rRNA m^5U747 (Madsen et al., 2003), respectively.

U1939 is located in a conserved region (1930–1970) in domain IV of 23S rRNA, which includes stem H70, the 1942 loop (containing U1939), stem H71, and the 1953 loop. In the crystal structure of the 70S ribosome, residues from this segment are seen to bridge with H44 of 16S rRNA through minor groove-minor groove interactions (Yusupov et al., 2001). Furthermore, the 1942 loop protrudes into the major groove of the acceptor stem of A site tRNA at the CCA tail. Structures of *Deinococcus radiodurans* 50S ribosome in complex with tRNA analogs (puromycin and sparsomycin derivatives and an acceptor arm mimic) (Bashan et al., 2003) show that the 1942 loop interacts with these tRNA analogs, suggesting an important role for this loop in A site tRNA binding. A cryo-EM structure of tmRNA in complex with the ribosome places the tmRNA in proximity to stem H71 (Valle et al., 2003). The ribosomal sequence between 1934 and 1949 is highly complementary (14 out of 16 nucleotides) to the sequence in the tRNA-like domain of tmRNA, strongly indicating that the 1942 loop has the potential to base pair with tmRNA. Although the role of methylation at U1939 is yet undetermined, its location in ribosome suggests that this modification may subtly modulate the binding of tRNA and/or tmRNA to the ribosome.

The m^5U MTase reaction has been studied primarily using TrmA, and a minimal mechanism has been proposed (Figure 1) (Kealey et al., 1994). In the first step, a cysteine nucleophile of the enzyme attacks C6 of uridine, forming an enolate (or equivalent enol) intermediate (2), which is in equilibrium with the off pathway 5,6-dihydropyrimidine intermediate (2a). C5 of the enolate intermediate is activated for electrophilic substitution. This is followed by the transfer of the methyl group of SAM to C5, generating a methylated protein-RNA intermediate (3). The final step involves a proton abstraction from C5 by a general base and β elimination of the enzyme. This catalytic mechanism resembles that of the reaction catalyzed by 5-methylcytosine (m^5C) MTase (Wu and Santi, 1985).

The recently reported crystal structure of apo-RumA displays a three-domain structure (Lee et al., 2004). The N-terminal domain is an OB fold, a five-stranded β barrel known to bind oligonucleotides/oligosaccharides. The central domain hosts a $[Fe_4S_4]$ cluster, rarely observed in SAM-dependent MTases. Based on the electrostatic potential surface and the location of the conserved positively charged residues, the central domain was proposed to be involved in RNA binding. The C-terminal domain is the catalytic domain and has the fold of a typical class I SAM-dependent MTase. Conserved sequence motifs in this domain have been iden-

*Correspondence: stroud@msg.ucsf.edu
[2]These authors made key contributions to the work.

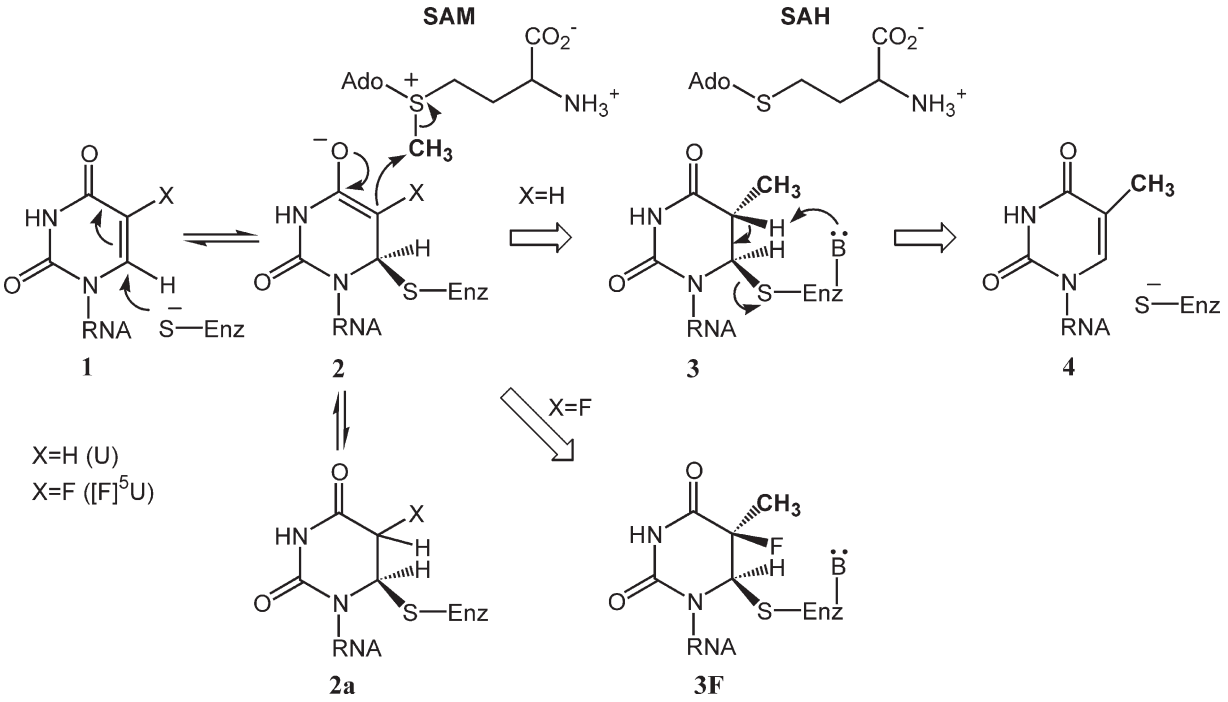

Figure 1. The Proposed Catalytic Mechanism of RNA m^{5}U MTases

tified, and their roles in cofactor binding and substrate specificity have been proposed (Lee et al., 2004).

Here we describe the X-ray crystal structure of the RumA-RNA-*S*-adenosylhomocysteine (SAH) ternary complex. This is the first RNA bound structure of a ribosomal RNA-modifying enzyme and of an RNA methyltransferase. The structure reveals that the bound RNA is folded into a unique conformation that allows the RNA to carry out functions that are usually performed by protein residues. Intra-RNA interactions facilitate flipping both the target base and a second base that participates in RNA-assisted cofactor binding. The unique quaternary interaction seen in the enzyme-RNA complex suggests a mechanism for achieving the selectivity of the enzyme for a single base within 23S ribosomal RNA. Interactions of the target base in the active site, along with our biochemical studies on specific mutant enzymes, identify key protein residues involved in the catalytic process, including residues responsible for base specificity and the general base catalyst. The position of the new methyl group suggests a mechanism to assist product release by steric clash.

Results and Discussion

Overview

The structure of a ternary complex containing RumA, SAH, and a covalently bound 23S rRNA fragment (1932–1968) with 5-fluoro-uridine ([F]^{5}U) at position 1939 was determined by molecular replacement methods. The structure of apo-RumA (Lee et al., 2004) was used as the search model. The structure was refined to 2.15 Å resolution to an R_{free} of 22.9% (Table 1). Each asymmetric unit contains two ternary complexes of RumA-RNA-cofactor. The structures of the two non-crystallographic symmetry (NCS)-related complexes are similar, with an rms deviation of 0.6 Å and 1.1 Å for proteins and RNAs, respectively.

The RNA in the RumA complex is folded into two structural elements and is bound at the concave sur-

Table 1. Crystallographic Refinement Statistics

	RumA-[F]RNA-SAH
Resolution (Å)	50 – 2.15
Space group	C2
z[a]	2
Unit cell dimensions (Å)	a = 190.1, b = 63.5, c = 112.0, β = 125.2°
Observed reflections	564191
Unique reflections	59466
R_{merge}[b]	8.9%(73.3%)[c]
I/σ(I)	12.7(1.9)[c]
Completeness	99.9%
Total atoms	8156
Water atoms	340
$R_{working}$[d]	17.4%
R_{free}[d]	22.9%
Rmsd bond lengths (Å)	0.021
Rmsd bond angles (°)	2.0

[a] z is the number of equivalent structures per asymmetric unit.
[b] $R_{merge} = \Sigma|I_{hkl} - \langle I_{hkl}\rangle|/\Sigma I_{hkl}$, where I_{hkl} is the measured intensity of hkl reflection and $\langle I_{hkl}\rangle$ is the mean of all measured intensity of hkl reflection.
[c] The values in parentheses are for the highest resolution bin (2.19 Å – 2.15 Å).
[d] $R_{working} = \Sigma_{hkl}||F_{obs}| - |F_{calc}||/\Sigma_{hkl}|F_{obs}|$, where F_{obs} is the observed structure factor amplitude and F_{calc} is the structure factor calculated from model. R_{free} is computed in the same manner as is $R_{working}$, with the test set of reflections (5%).

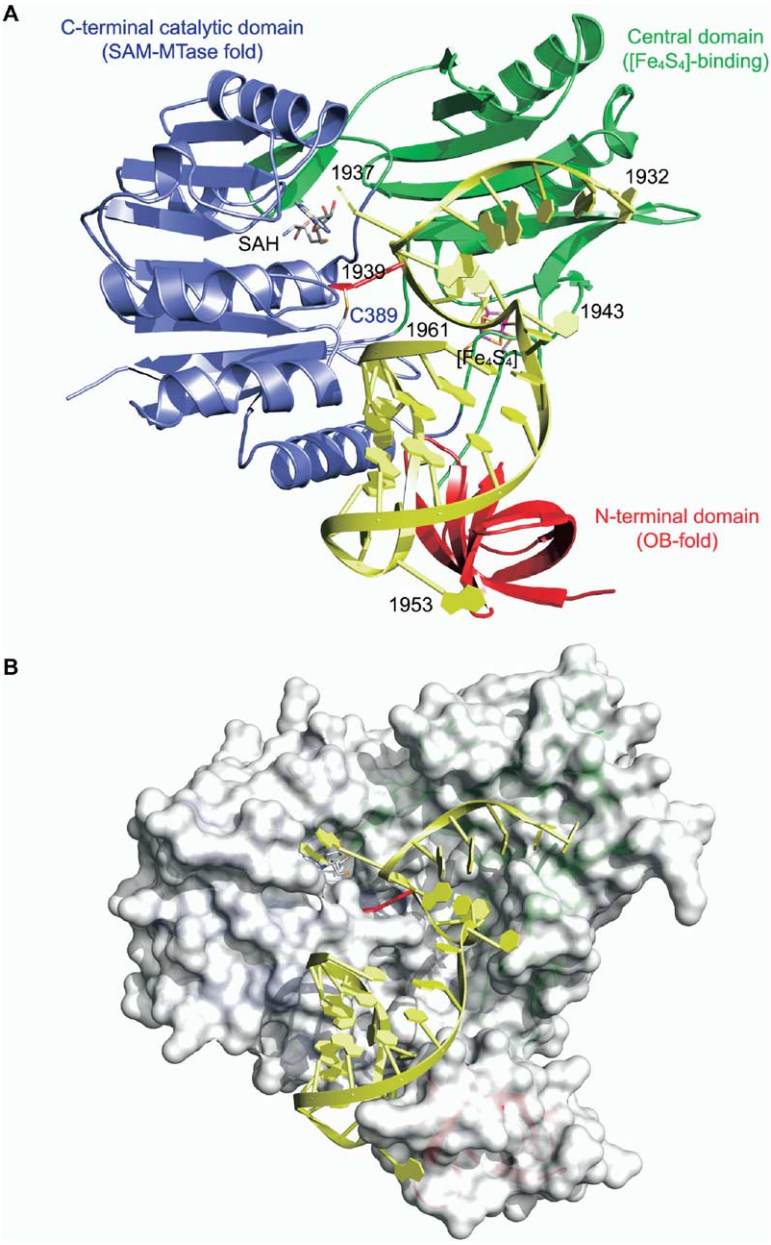

Figure 2. Overall Structure of the RumA-RNA-SAH Complex

(A) Ribbon representation of the complex. The N-terminal, central, and C-terminal domains of RumA are colored in red, green, and blue, respectively. The observed RNA, corresponding to 1932–1961 of *E. coli* 23S rRNA, is colored yellow, with the exception of U1939, which is colored red. SAH, the catalytic cysteine (C389) and the $[Fe_4S_4]$ cluster, and the side chains of its coordinating cysteines are shown in sticks (silver for C, red for O, blue for N, orange for S, and magenta for Fe).

(B) Surface representation of RumA. The orientation shown in (A) is rotated by 25° along the y axis to illustrate the binding groove. The molecular suface of RumA is colored white. The ribbon colors are the same as in (A).

face formed by the three domains of RumA (Figure 2). The 5′ end (1932–1943) containing the target nucleotide U1939 forms a compact folded loop, whereas the 3′ segment (1944–1961) is a canonical hairpin. The 5′ end loop and the 3′ hairpin do not have any mutual tertiary interaction. The extreme 3′ segment (1962–1968) is not observed in our structure. Formation of the protein-RNA complex results in 2709 $Å^2$ buried surface area, accounting for 38% of the RNA surface.

Unusual Fold of the 5′ End Loop and Its Contribution to Nucleotide Flipping and Substrate Selectivity

The 5′ end loop (1932–1943) binds at the groove formed by the central and the catalytic domains of RumA. Compared to other protein bound single-stranded RNA segments (Antson, 2000), the fold of the 5′ end loop is strikingly intricate and compact. The fold and intra-RNA interactions of this loop in the RumA complex are very different from those observed in the corresponding segment in the 50S ribosome from *Deinococcus radiodurans* that has the identical sequence (Bashan et al., 2003) (Figures 3A and 3B). Except for A1937 and U1939, which are flipped out of the loop, all the residues of the 5′ end loop bind to the central domain, with the bases clustered at the concave side of the curved sugar phosphate backbone (Figures 2 and 3B). The 5′ end loop contains two base stacks (Figure 4A). Residues 1932–1936 form an inline coaxial five-layered base stack that interacts with residues in the core β sheet in the central domain. Following the 1932–1936 stack, the backbone bends abruptly at 1937 and initiates the second base stack that contains four layers in

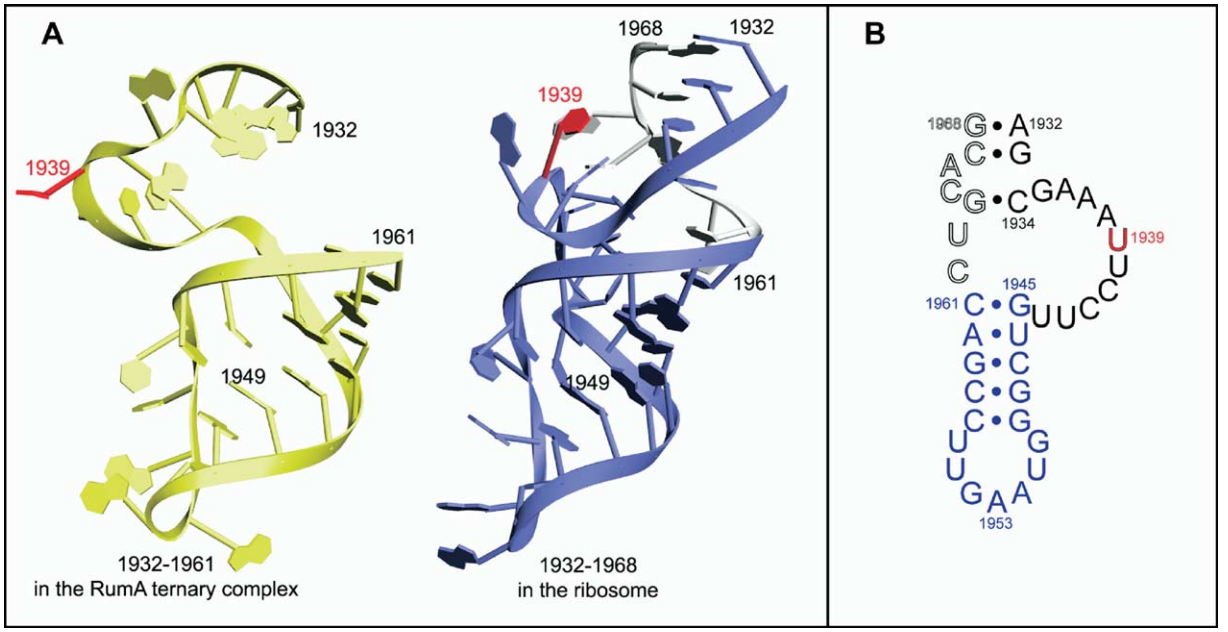

Figure 3. Structural Comparison of the RumA Substrate in the Cocrystal Structure and that in Ribosome

The structure of the 1932–1968 segment has a well-conserved fold in the ribosome (Ban et al., 2000; Bashan et al., 2003; Yusupov et al., 2001), and it is represented by the *Deinococcus radiodurans* structure in this comparison. The nucleotide sequence of this segment in *E. coli* is identical to that in *Deinococcus radiodurans*.

(A) Side-by-side view of the RumA substrate in the cocrystal structure (yellow, left) with the analogous residues in the ribosome (blue, right). The structure was rotated by 60° from the orientation shown in Figure 2. The backbones of the hairpins are well aligned, whereas the backbones of the 5′ end loops deviate significantly from each other. The extreme 3′ segment (colored silver), which is not observed in the RumA cocrystal structure, makes three base pairs with the 5′ end segment in the ribosome.

(B) Secondary structure of 1932–1968 (*E. coli* numbering) of the 23S rRNA. The 5′ segment is colored black, and the hairpin is colored blue. U1939 is colored red. The extreme 3′ segment (1962–1968) was not observed in the RumA-RNA complex and is shown in open letters.

nonsequential order: 1938-1942-1941-1940. This stack is almost perpendicular to the 1932–1936 stack and is vertically inserted into a deep crevice in the protein surface that reaches the [Fe_4S_4] binding site.

Nucleotide flipping is a common strategy used in nucleic acid-modifying enzymes for the bases to gain access to the active site (Roberts and Cheng, 1998). It is an energetically expensive process, since it involves disruption of favorable interactions, such as base stacking and hydrogen bonds, and generates a cavity in the hydrophobic core of the nucleic acid. In many nucleic acid-modifying enzymes, protein residues are inserted into the cavity to provide compensating favorable interactions and balance the free energy cost of extracting the base for binding and catalysis (Hoang and Ferré-D'Amaré, 2001; Klimasauskas et al., 1994; Slupphaug et al., 1996). In the RumA complex, no protein residue is inserted into the sites vacated by eversion of U1939 and A1937. Instead, the RNA chain following U1940 folds back, and two RNA nucleotides, C1941 and C1942, occupy the site vacated by the flipping of U1939 and stack between A1938 and U1940 (Figures 4A and 4B). This insertion of surrogate nucleotides in the RNA core provides energetically favorable stacking and van der Waals interactions and is reminiscent of the insertion of protein residues seen in other nucleotide flipping systems.

To assess the importance of this base stacking, we measured the methylation activity on a 37-mer RNA (1932–1968) with a riboabasic modification at C1942 (C1942rab). The wild-type 37-mer has a specific activity of 2.2×10^3 mmole/min/mole. In contrast, no detectable methylation activity was obtained when the C1942rab RNA was used as a substrate. That is, the activity toward the abasic RNA is at least 1000-fold lower than the activity with the wild-type substrate, as inferred from the detection limit of our assay. This result supports the crucial role of the interaction provided by the inserted C1942 base in the productive folding of the substrate.

The flipping of A1937 is stabilized by van der Waals interaction between the A1938 base and the A1936 ribose that results from the sharp bending of the RNA backbone at A1937. A base-specific hydrogen bonding network involving G1935, A1938, and the phosphate moiety of U1943 helps stabilize the unusual RNA conformation (Figure 4B). This hydrogen bonding network connects the two base stacks, maintains 1937-1938-1939 in the zig-zag geometry, and ensures the nonsequential stacking order of 1938-1942-1941-1940. Thus, the unusual fold is stabilized by a specific set of intra-RNA interactions that are not typically seen in single-stranded RNAs.

The conformation of the 5′ end loop and the flipping of the bases is also guided by the complementary protein surface. Specific interactions with protein residues

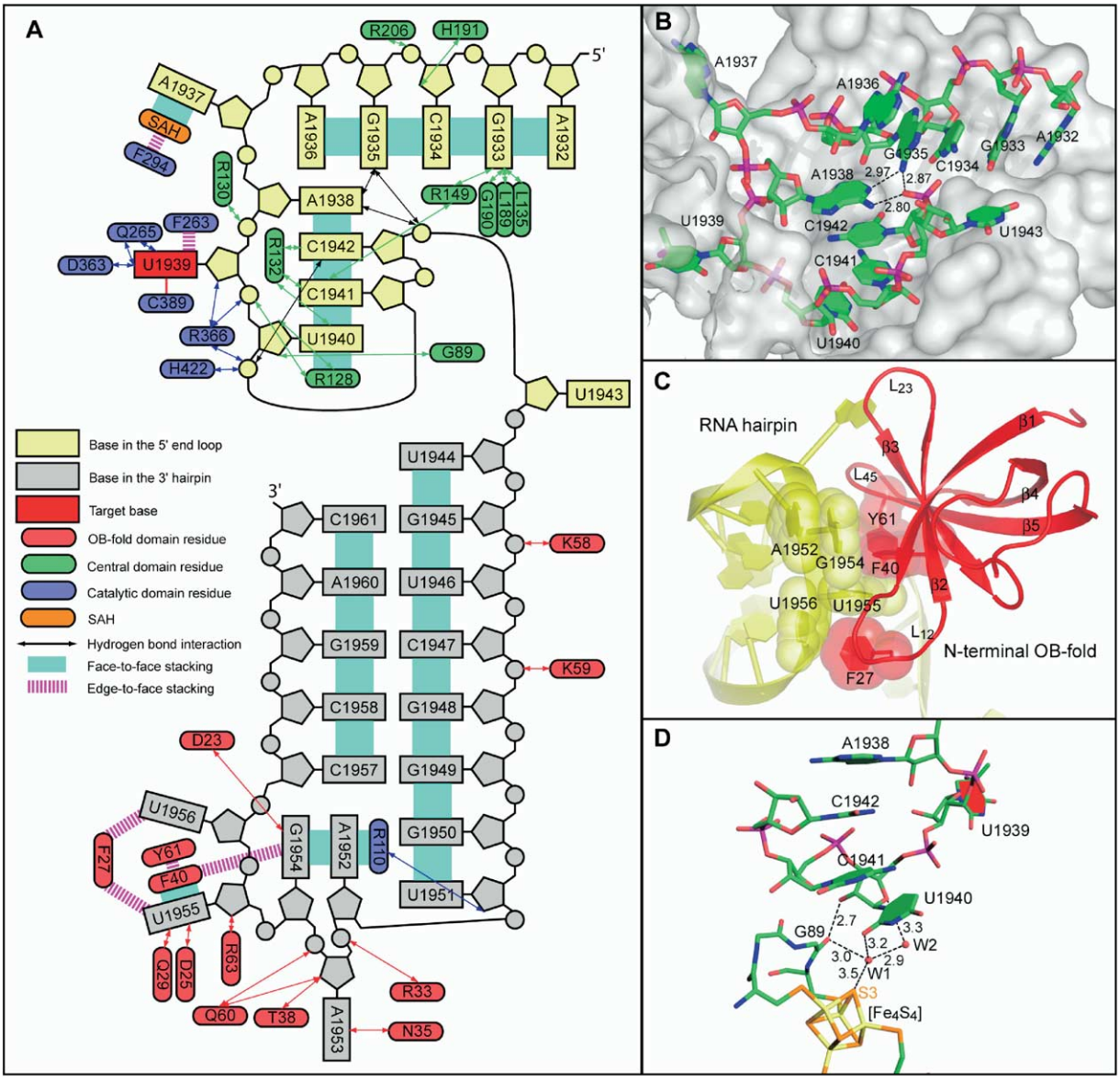

Figure 4. Interactions between RumA and Its Substrate RNA

(A) Diagram of the secondary structure and interactions of the bound RNA.

(B) Base stacking and intra-RNA hydrogen bond network in the 5′ end loop. C1941 and C1942 occupy the space vacated by the flipped-out U1939 and provide stacking interactions with A1938 and U1940. G1935, A1938, and U1943 form a closed hydrogen bonding network that stabilizes the base flipping. The molecular surface of RumA is shown, and the RNA is shown in a stick model (green for C, red for O, blue for N, and magenta for P).

(C) Recognition of the hairpin by the N-terminal OB fold. RumA and RNA are colored red and yellow, respectively. The protein and RNA residues involved in an aromatic interaction network are displayed in a transparent space-filling model.

(D) Interactions between the [Fe_4S_4] cluster and RNA through a water-mediated hydrogen bonding network. Elements are colored as follows: green for C, red for O, blue for N, magenta for P, orange for S, and yellow for Fe. The hydrogen bonds are shown in black dashed lines.

help stabilize the nonsequential stack: R132 and R149 hydrogen bond to bases U1940, C1941, and C1942 in the stack, and R128 extends the stacking at U1940 (Figure 4A). Several additional hydrogen bonds are formed between the central domain and the sequential base stack (1932–1936), and amino acid side chains from the catalytic domain make specific contacts with the flipped bases. These protein-RNA interactions, as well as the intra-RNA interactions, are possible only when the RNA is folded into the observed conformation. Thus, the folding of the 5′ end loop is not only necessary for presenting bases to the active site, it also provides a mechanism for selectivity of the enzyme.

The Preformed Hairpin Binds to the OB Fold and Enhances the Catalytic Efficiency

In the RumA-RNA complex structure, residues 1945–1961 form a five base-paired hairpin with a seven base

internal loop (1950–1956). Residue 1944 stacks against 1945 but is not base paired (Figure 4A). The rmsd of the phosphorus atoms between the hairpin in the 50S ribosome from *Deinococcus radiodurans* (Bashan et al., 2003) and that in the RumA complex is 2.2 Å (Figure 3B), suggesting that conformation of the backbone remains largely unaltered upon RumA binding. The hairpin binds in the cleft formed between the N-terminal OB fold domain and the catalytic domain, with the OB fold domain providing most of the contacts to the hairpin (Figure 4A). There are very few interactions between the stem of the hairpin and the protein, and the OB fold domain recognizes the RNA hairpin mainly through interactions with the internal loop nucleotides (Figures 4A and 4C). The binding surface of the RumA OB fold is comprised of strands β2, β3, and the C-terminal segment of β1, and loops L_{12}, L_{23}, and L_{45} form clamps to bind the RNA. Several polar residues from the RumA OB fold make hydrogen bonds and electrostatic interactions with A1953, G1954, and U1955. Four RNA bases of the internal loop (A1952, G1954, U1955, and U1956) and three aromatic protein side chains (F27, F40, and Y61) form an extended network of aromatic interactions, involving both face-to-face and face-to-edge stacking (Figure 4C).

The ligand binding surface of an OB fold is universal, although there is no sequence homology among OB folds (Arcus, 2002; Murzin, 1993; Suck, 1997) (Figure 4C). The N-terminal domain of aspartyl-tRNA synthetase is another RNA loop binding OB fold. It recognizes the anticodon loop of $tRNA^{asp}$ using the same ligand binding face as that in the RumA OB fold (Eiler et al., 1999; Ruff et al., 1991). However, the nucleotide sequence and detailed interactions are very different from those seen in the RumA complex structure. The RumA-RNA complex supports the argument that the OB fold is a versatile binding domain that can adapt to various ligands.

The 3′ hairpin binds distant from the active site of RumA and does not have any tertiary interaction with the 5′ region. In order to assess the contribution of the hairpin segment to catalysis, we measured the enzymatic activity of RumA for the 37-mer RNA (1932–1968) and for a 12-mer 5′ segment (1932–1943) lacking the hairpin. The k_{cat}s for RumA on the 37-mer substrate and the 12-mer are 0.18 s^{-1} and 0.006 s^{-1}, respectively, and the K_ms are 9.2 μM and 34 μM, respectively. This represents a 30-fold higher k_{cat} and a 3.7-fold lower K_m for the 37-mer. Thus, the presence of the hairpin results in a 110-fold higher catalytic efficiency (k_{cat}/K_m). The effect on k_{cat} is 8-fold greater than the effect on K_m, suggesting that the binding energy contributed by the hairpin is realized predominantly in the transition state complex (Fersht, 1999). The binding of the hairpin therefore appears to stabilize the productive alignment of catalytic residues in the transition state, resulting in a higher catalytic rate.

RNA-Induced Conformational Change in RumA

In order to evaluate the structural changes between apo and substrate RNA-bound RumA, we determined the Cαs whose positions are unchanged relative to each other in the two structures by difference distance matrix calculation (Perry et al., 1990). Three discreet structural cores were identified which correspond to the three RumA domains, suggesting that upon binding RNA, each domain undergoes a movement that is independent of the other two domains. Separate alignments using individual domains revealed that all three domains move toward the bound RNA in a "hinged" motion, which results in the change of the shape of the binding surface that accommodates the RNA. In particular, the central domain and the catalytic domain rotate toward each other by about 7° along their interdomain hinge. The N-terminal OB fold swings by about 10° toward the catalytic domain to lock in the hairpin. In addition to the domain movements, structural changes are also observed within each domain.

The conformational changes of the active site residues were evaluated by aligning the catalytic domains. Many residues exhibit movement toward the target uridine and the cofactor (Figure 5). The shifts of Cα atoms in most residues are less than 1 Å. F263 and Q265 move by a large distance of 2.5 Å and 1.9 Å, respectively. In addition, the side chains of E424 and R366 swing by 58° and 53°, respectively, to interact with U1939 (Figure 5). The concerted movement of the active site residues results in the active site closure.

Involvement of [Fe_4S_4] Cluster in RNA Binding

The iron-sulfur cluster in the RumA complex structure interacts with the RNA through water-mediated hydrogen bonding (Figure 4D). A water molecule (W1) bridges O2 of U1940 (the bottom layer of the nonsequential base stack) and S3 of [Fe_4S_4]. W1 also hydrogen bonds to O4′ of U1940 through a second water (W2). In addition, the carbonyl oxygen of G89, a residue proximal to the cluster, hydrogen bonds to W1 and the 2′ hydroxyl of U1940. G89 is completely conserved among RumA orthologs, and any side chain at position 89 would affect the hydrogen bonding network by creating steric hindrance. The U1940-containing stack is the most ordered RNA segment in the crystal structure as revealed by the low temperature factors, suggesting that the conserved [Fe_4S_4] and G89 might serve as the platform for binding U1940 to initiate the overall binding process.

The iron-sulfur cluster is unlikely to participate directly in catalysis in RumA, since it is absent in homologous m^5U MTases. Like RumA, endonuclease III possesses a [Fe_4S_4] cluster that does not participate in catalysis. It has been proposed to have a role in maintaining the fold of a DNA binding domain (Fromme and Verdine, 2003). Recent data from our lab show that the RumA cluster can be oxidized under conditions that might exist during physiological oxidative stress, but the oxidation is accompanied by decomposition of the cluster and protein precipitation (Agarwalla et al., 2004). This observation and the interactions in the RumA-RNA structure suggest that the iron-sulfur cluster of RumA may have an important role in stabilizing the structure of the central domain.

Substrate-Assisted Cofactor Binding

The catalytic domain displays a typical SAM binding fold utilizing some interactions that are conserved in

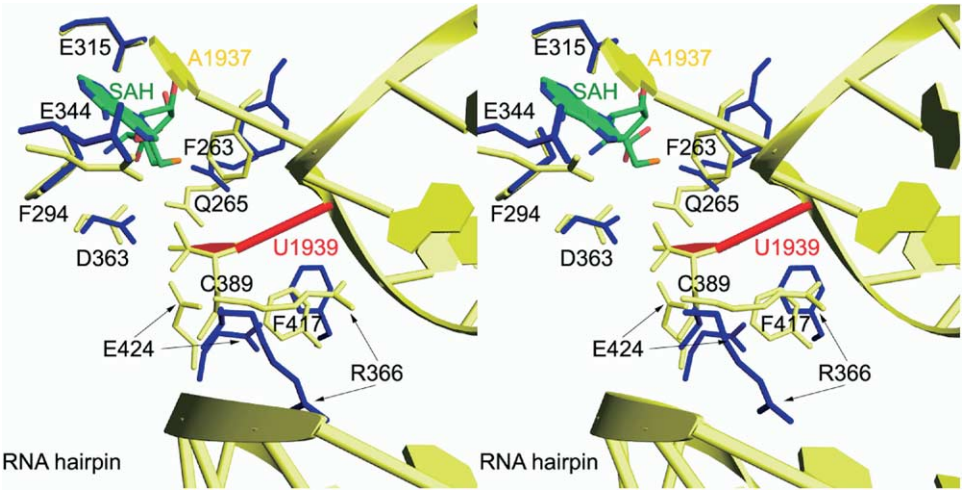

Figure 5. Stereoview of Conformational Change of RumA upon Binding to RNA

The structures of RumA in the presence and absence of RNA are colored yellow and blue, respectively. SAH is colored green. The structures are superimposed by aligning the Cα atoms of residues in the catalytic domain using the LSQKAB program in the CCP4 package (CCP4, 1994; Kabsch, 1976).

other SAM-dependent MTases (Lee et al., 2004; Malone et al., 1995) (Figure 2). However, the RumA complex displays a novel utilization of the substrate in assisting the binding of the cofactor (Figures 4A and 5 and see Figure S1A in the Supplemental Data available with this article online). In several SAM-MTases, the adenine ring of the cofactor is packed between aromatic/hydrophobic side chains (Malone et al., 1995). For example, in the M. HhaI-DNA-SAH complex, W41 makes a face-to-face and F18 makes an edge-to-face stacking interaction to the cofactor from either face of the adenine ring (Klimasauskas et al., 1994) (Figure S1B). In the RumA complex, the flipped-out A1937 of the substrate RNA makes a face-to-face stacking interaction with the adenine ring of SAH, thus performing a role analogous to W41 of M. HhaI. This stacking shields the cofactor from solvent. To complete the packing, the conserved F294 makes an edge-to-face interaction with SAH from the other side relative to A1937, similar to F18 of M. HhaI. Thus, in the RumA complex, A1937 is recruited to perform the function that is performed by a protein residue in many other SAM-MTases. This dramatic reorientation of a nucleotide to bind the cofactor has not been documented before.

To evaluate the contribution of this novel interaction on the methylation reaction, we measured the activity of RumA toward the 37-mer substrate (1932–1968) with a riboabasic modification at A1937 (A1937rab). Because the base of the flipped-out adenine interacts almost exclusively with the cofactor, it is unlikely that the A1937rab modification alters the overall fold of the RNA and the flipping of U1939. The elimination of the stacking interaction from A1937 is expected to destabilize the cofactor binding and result in decreased methylation activity. The K_ms for SAM on the wild-type and the A1937rab substrates are 29 μM and 134 μM, respectively, and the k_{cat}s are 0.18 s^{-1} and 0.042 s^{-1}, respectively. This is a 4.6-fold increase in K_m, a 4.3-fold decrease in k_{cat}, which represents a 20-fold decrease in the catalytic efficiency (k_{cat}/K_m) with respect to SAM as a result of the abasic modification. This corresponds to an activation energy of 1.8 kcal/mole, which matches well the free energy of stacking two adenine bases in aqueous solution (1.5 kcal/mole) (Solie and Schellman, 1968). Thus, the binding energy of stacking between A1937 and the cofactor in the wild-type substrate is utilized to lower the activation energy and thereby enhance catalysis. This result supports an important role of A1937 in cofactor binding and orientation for catalysis.

Conformation and Interactions of U1939 in the Active Site

The U1939 base adopts a half-chair conformation, in which C5 and C6 are out of the plane with C5 pointing toward SAH and C6 pointing toward the catalytic cysteine C389 (Figure 6). The electron density shows that C6 is covalently attached to C389-SG through a thioether linkage (Figure 6A). C5 is sp^3 hybridized and is attached to both the fluorine and the transferred methyl group, and clear electron density is observed for both groups. Since both groups have nine electrons each and are symmetrically distributed around C5, their identities were assigned assuming that the density proximal to SAH corresponds to the transferred methyl group. The methyl group and SD of SAH are 3.3 Å apart, and there is no electron density between the two atoms, indicating that methyl transfer is complete (Figure 6). The completed methyl transfer, together with the covalent bond between the C6 and C389-SG, suggest that the structure is the trapped intermediate 3F (Figure 1).

The flipped-out uridine is stabilized by interactions that are provided by residues conserved in m5U MTases. F263 forms an edge-to-face aromatic interaction with the uracil ring and is itself held by the sugar-phosphate backbone of U1939 and the methionine moi-

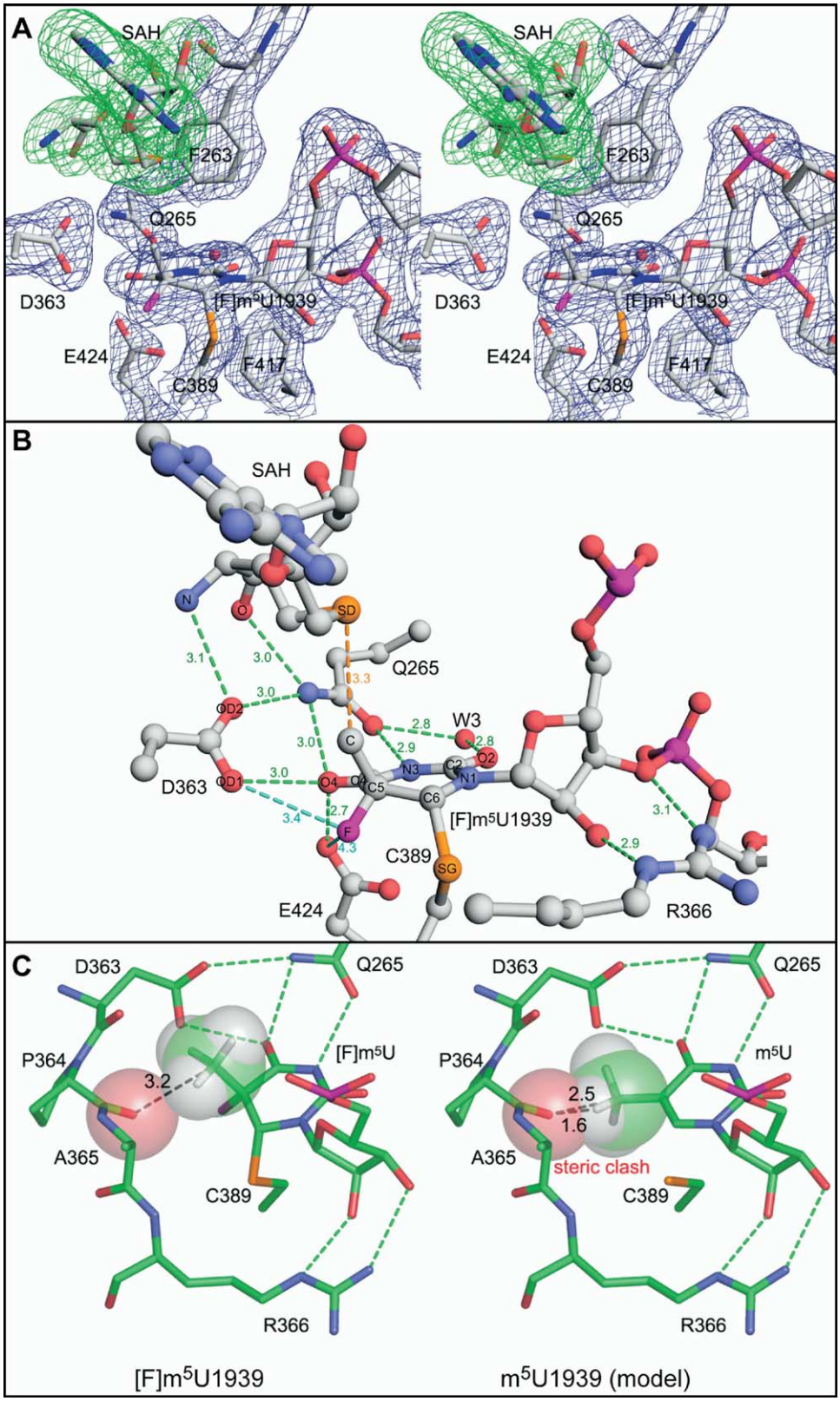

Figure 6. The Active Site of RumA

(A) Stereoview of the sigma weighted $2F_o - F_c$ electron density at the active site. The map was contoured at 1.2 σ and colored green for SAH and blue for the remaining region. The map shows the linkage between C389-SG and U1939-C6 and no continuous density between SAH and U1939. The densities of the fluorine and methyl group are evenly distributed around U1939-C5.

ety of SAH (Figure 6A and Figure S1A). F417 contacts the uracil ring through van der Waals interaction from the opposite side relative to F263. These two phenyl rings sandwich the uracil base, preventing it from moving along the axis perpendicular to the plane of the base. The guanidino group of R366 hydrogen bonds to O2′ and O3′ of U1939. The U1939 base; the side chains of residues Q265, D363, and E424; and a water molecule (W3) form an intricate hydrogen bonding network (Figure 6B). These interactions together hold the flipped-out U1939 in the productive conformation. Q265, D363, and E424 possess hydrogen bonding and proton transfer abilities and directly contact the target uracil. In order to investigate the functional roles of these residues, we constructed conservative mutants (Q265E, D363N, and E424Q) and also made alanine mutants at each of these three positions.

Q265 in Uracil Recognition

RumA is not only site specific, it is also base specific; a U1939C mutant 23S rRNA is not methylated (Agarwalla et al., 2002), despite similar chemistry involved in the catalytic mechanism. Hydrogen bonding between N3 and O4/N4, the two atoms that differentiate uracil from cytosine, and protein side chains having amide or carboxyl groups are often employed for discrimination of the two pyrimidine bases by proteins (Liu and Santi, 1992). Q265 in the RumA complex forms bidentate hydrogen bonds to N3 and O4 of U1939 (Figure 6B). Hence, it is well positioned to be the primary uracil-recognizing residue. Q265-NH_2 is also a hydrogen bond donor to the carboxylate of D363, and a water (W3) bridges Q265-OE1 and U1939-O2. These latter interactions maintain Q265 in the proper orientation for interaction with the uracil base. In addition, Q265 is a hydrogen bond donor to the carboxylate of the methionine moiety of the cofactor, suggesting a role of Q265 in SAM binding as well. The Q265A mutant enzyme displays a specific activity of 3.6 mmole/min/mole, 830-fold lower than that of the wild-type enzyme (3.0×10^3 mmole/min/mole), whereas the Q265E mutant has no detectable activity. Thus, not only is the hydrogen bonding capability of Q265 required, but the very specific hydrogen bonding character of an amide is required at this position.

Multiple Roles of D363

D363 interacts with several functional groups in the active site, including U1939, SAH, and Q265 (Figure 6B). Based on these interactions, D363 may contribute to the binding of the cofactor, orientating Q265 and stabilizing the enolate intermediate 2. In addition, D363 is proximal to the fluorine attached to C5 (3.4 Å) and hence might serve as the general base required for abstraction of the C5 proton after the methyl transfer (intermediate 3). The D363A mutation resulted in complete loss of activity, whereas the D363N mutant enzyme had only 2-fold lower specific activity (1.5×10^3 mmole/min/mole) than the wild-type enzyme. The hydrogen-bonding functions are retained in the D363N mutant, but the proton transfer character is lost. The retention of high activity by D363N eliminates D363 as the general base in the reaction; however, the loss of activity by D363A indicates the importance of retaining hydrogen-bonding capability at this position.

E424 Is the General Base

E424 is within hydrogen bonding distance of O4 of the target uridine and also is proximal to the C5 fluorine (4.3 Å, Figure 6B). Hence, it is in a position to stabilize the enolate intermediate 2, and/or it can be the general base for abstracting proton from intermediate 3. The specific activity of the E424A mutant is 1200-fold lower than the wild-type enzyme, indicative of an important role of this residue. The E424Q mutant displays a biphasic reaction profile with an initial burst phase followed by a slow second phase (Figure S2A). The magnitude of the initial burst in the reactions is comparable to the concentration of the enzyme used. This kinetic behavior is characteristic of the accumulation of an enzyme bound intermediate during the reaction (Hartley and Kilby, 1954). In contrast, both the wild-type enzyme and the mutant enzyme with significant activity (D363N) display linear reaction profiles (data not shown). For the E424Q mutant, the biphasic kinetic behavior can be explained by a fast methyl transfer step followed by the slow resolution of intermediate 3 (Figure 1). Thus, in the E424Q mutant, proton abstraction and β elimination become the rate-limiting step of catalysis. In this mutant enzyme, the rate constant of proton abstraction as determined from the slope of the second phase is 4.5×10^{-4} s^{-1}. Although the same constant cannot be determined for the wild-type protein, the absence of a second phase indicates that it is considerably faster than k_{cat}, i.e., 0.18 s^{-1}. Therefore, the E424Q mutation results in at least a 350-fold reduction in the rate of proton abstraction.

The trapping of intermediate 3 by the E424Q mutation was further confirmed by SDS-PAGE analysis. In the absence of SAM, wild-type RumA shows a stable RNA-protein complex band that was interpreted as the off-pathway intermediate 2a (Figure S2B, lane 1). This interpretation is based on a detailed analysis of the mechanistically similar TrmA (Gu and Santi, 1992). In the presence of SAM, the wild-type enzyme efficiently turns over and does not form a stable covalent com-

(B) Interactions between amino acid side chains, the target uridine, and SAH. Possible hydrogen bonds are represented by green dashed lines. Distances between the C5 fluorine and the two general base candidates D363 and E424 are shown as cyan dashed lines. The distance between SAH-SD and the C5 methyl group, shown as a yellow dashed line, suggests the completion of methyl transfer.

(C) Proposed mechanism of product release illustrated by a side-by-side view of the structure of [F]m^{5}U1939 and a model of m^{5}U1939 in the active site. The van der Waals spheres are shown for P364-O and the C5 methyl group. The radii used here are 1.52 Å for O, 1.7 Å for C, and 1.2 Å for H. (Left) Covalent intermediate 3F as seen in the crystal structure. C5 is sp^3 hybridized. (Right) A model of the final product after β elimination and C5=C6 double-bond formation. C5 is sp^2-hybridized, and the methyl group is coplanar to the uracil. Steric clash is visible between P364-O and the C5 methyl group.

plex (Figure S2B, lane 2). In contrast, the E424Q mutant does not form a stable complex in absence of SAM (Figure S2B, lane 3) suggesting that this mutation affects the relative stability of intermediates 2 and 2a, possibly by changing the local electrostatic environment. However, a stable RNA-protein complex is trapped in the presence of SAM (Figure S2B, lane 4). This complex is very likely the methylated intermediate 3. These gel-shift experiments together with the kinetic data prove that E424 is the general base in the β elimination step.

Mechanism of Product Release

The conformation of U1939 and its contact with amino acids in the active site suggest a possible mechanism of product release. After the last step of catalysis (β elimination) is complete, the C5=C6 double bond is formed, and the m^5U1939 base has a planar conformation in which the C5 is sp^2 hybridized and the new methyl group is in plane with the pyrimidine ring (Figure 6C). However, such a conformation would place the C5 methyl group in unfavorably close contact to the main chain oxygen of P364 (2.5 Å between P364-O and the carbon of the methyl group and 1.6 Å between the P364-O and the most proximal hydrogen of the methyl group). P364 is in the highly conserved motif IV (DPXR) of m^5U MTases, and we have proposed that the torsional constraint conferred by proline would be important to catalytic function (Lee et al., 2004). The van der Waals repulsion between the C5 methyl group and the P364-O would incur a conformational change in the P364-containing loop and/or in the position of m^5U1939, which in turn might disrupt the hydrogen bonds from D363 and R366 and promote product release. A similar mechanism has been proposed for M. HhaI DNA m^5C MTase, in which steric clash is expected between the planar C5 methyl group and a different proline in motif IV (O'Gara et al., 1996). The almost universal existence of a proline in motif IV of DNA and RNA MTases (Anantharaman et al., 2002; Malone et al., 1995) suggests that steric clash resulting from the torsional constraint conferred by a critically placed proline may be a general mechanism of product release in this group of enzymes.

Conclusions

A primary issue is how RNA-modifying enzymes gain unique specificity for a single RNA base within the entire RNA complement of the cell. Two structures of enzymes that modify nucleotides in folded RNAs in complex with their RNA substrate have so far been described: pseudouridine synthase TruB modifies U55 in the preformed T stem-loop of tRNA (Hoang and Ferré-D'Amaré, 2001; Pan et al., 2003). Archaeosine tRNA-guanine transglycosylase modifies G15 in the folded λ form of tRNA (Ishitani et al., 2003). In contrast, many modified nucleotides in the ribosome, including U1939, are located in buried loop or bulge regions, and modifications of these bases most probably occur before or during ribosome assembly when the loops or bulges are unstructured or are partially folded. The RumA complex provides the first insight into this process. Instead of adopting an extended structure, the single-stranded substrate in the complex is refolded on the enzyme into a compact conformation with many intra-RNA interactions. The refolding thereby provides a mechanism for dynamic structure-specific recognition of the single target base in ribosomal RNA. Thus, it is not only the sequence that is recognized by the enzyme but also the ability of the RNA to conform to the specified conformation utilizing intra-RNA constraints that is in turn determined indirectly by the RNA sequence. This mechanism of selectivity that depends on the ability of the enzyme-RNA complex to reach a unique quaternary interaction, as well as sequence specific contacts, may be utilized by other enzymes that modify single-stranded nucleic acids. A similar "self-recognition" mechanism is employed by the Pot1 end-capping protein that binds telomeric single-stranded DNA, where the tertiary intra-DNA interactions in the compact folded DNA are essential for specificity (Lei et al., 2003). Although not directly analogous, the recently reported structure of the CCA-adding enzyme/tRNA complex provides another example of an RNA that participates in the enzymatic reaction, in this case by providing part of the template for the incoming base (Xiong and Steitz, 2004).

The particular RumA RNA substrate participates at various levels in the catalytic process. Access to the target base remains a predominant function of nucleotide flipping out from its normal secondary structure in enzyme-nucleic acid complexes (Roberts and Cheng, 1998). The RumA-RNA complex structure extends the functional repertoire of this mechanism by flipping a second nucleotide (A1937) that participates in binding the cofactor. Cheng and Blumenthal (2002) had proposed that base flipping in RNA may play roles that are not observed in DNA, and the RumA structure validates this proposition. Several intra-RNA interactions including a hydrogen bonding network involving three nucleotides and the insertion of two nucleotides into the void generated by base flipping provide the compensating free energy required for flipping. The 3′ hairpin region of the substrate RNA, even though it does not interact with the protein active site, interacts with another domain of the protein to provide binding energy. This region increases selectivity and catalytic efficiency (k_{cat}/K_m).

It has been proposed that the primordial RNA world first evolved to an RNA-protein environment before the development of the extant life forms (Freeland et al., 1999). It is conceivable that early protein enzymes had not acquired sufficient proficiency and required the support of RNA molecules for augmenting their function. The active participation of the substrate RNA in RumA catalysis is certainly consistent with this conjecture. The rumA gene is widespread throughout the eubacterial kingdom (Agarwalla et al., 2004), indicating an early evolutionary origin for RumA. We therefore speculate that RumA and its substrate have preserved features from the early RNA-protein era.

Experimental Procedures

Preparation and Crystallization of RumA-RNA-Cofactor Complex

E. coli RumA was cloned, expressed, and purified as described (Agarwalla et al., 2002). The 23S rRNA fragment 1932–1968 with

[F]^{5}U1939 modification was purchased from Dharmacon, Inc. The enzyme-substrate covalent intermediate was formed by incubating 50 μM RumA with equimolar [F]^{5}U RNA in 50 mM Tris-HCl (pH 7.5) containing 1 mM $MgCl_2$, 5 mM DTT, and 2.5 mM SAM at room temperature for 1 hr. The reaction mixture was then applied to a HiTrap Q column (Pharmacia) equilibrated with 20 mM Tris-HCl and 100 mM NaCl (pH 7.5). Separation was performed using a gradient from 100 mM NaCl to 550 mM NaCl. The fractions containing the complex, as judged by SDS-PAGE analysis, were pooled and concentrated. The purified complex was dialyzed against 20 mM Tris-HCl and 50 mM NaCl (pH 7.5). Crystals were grown using the hanging drop vapor diffusion method. A solution containing 3 mg/mL purified complex and 1 mM SAM was mixed with an equal volume of well buffer (100 mM sodium cacodylate [pH 6.5], 1.5 M ammonium sulfate, and 10 mM $MgCl_2$).

Data Collection and Structure Determination

Crystals were transferred to the well buffer solution containing 20% (w/v) glucose shortly before immersion in liquid nitrogen. Diffraction data were collected on frozen crystals at the Advance Light Source (ALS, Lawrence Berkeley Lab, CA), beamline 8.3.1. Data were processed and scaled using DENZO and SCALEPACK (Otwinowski and Minor, 1997).

The structure was determined by the molecular replacement method using apo RumA as the search model (Lee et al., 2004). Solutions for both protein molecules in the asymmetric unit were obtained with CNS (Brunger et al., 1998) and were used to calculate the initial density map. The cofactor in the complex crystal was identified as SAH according to the lack of electron density for the epsilon methyl group, even though SAM was added in the crystallization drop. The cofactor product SAH might have remained trapped in the protein-RNA complex after the methyl group was transferred to U1939. It is also possible that it was present in the added SAM, since commercial preparations of SAM are known to contain SAH as a contaminant (Hoffman, 1986). The RNA model was progressively built into the density as the iterative refinement proceeded. Model building of the RNA and rebuilding of the protein were carried out using Quanta (Accelrys, San Diego, CA) and were assisted by improved maps using ARP/wARP (Perrakis et al., 1999). Refinement was carried out using REFMAC5 (CCP4, 1994; Murshudov et al., 1997). The three protein domains and RNA molecules were each treated as separate TLS groups (Winn et al., 2001), and NCS restraints were not applied during the refinement. The stereochemical quality of the final structure was verified by PROCHECK (Laskowski et al., 1993). Structual figures were prepared using PyMOL (DeLano Scientific) and Ribbons (Carson, 1997).

Subcloning and Mutagenesis of RumA

We subcloned the rumA gene into a construct that would provide a $(His)_6$-tag protein, thereby eliminating copurification of endogenous RumA during the purification of mutant enzymes. The rumA gene was amplified from the vector pRjr (Agarwalla et al., 2002) using the N-terminal primer 5′-GGAATTCCATATGGCGCAATTCTACTCTG CAAAACG-3′ and C-terminal primer 5′-GCGGATCCTATTTAACG CGCGAGAAAAGTACCATCGATTC-3′. The PCR product was digested with NdeI and BamHI and ligated with similarly restricted plasmid pET-28b. The ligated product was transformed into *E. coli* DH5α. The resultant construct, pET28-RumA, was confirmed by DNA sequencing. Site directed mutagenesis was performed by QuikChange Kit (Stratagene) using the appropriate mutagenic primers. All mutant sequences were confirmed by DNA sequencing.

Purification and Characterization of $(His)_6$-Tag RumA

The construct pET-28 RumA was transformed into *E. coli* BL21(DE3) plysS cells. The transformed cells were grown in M9 minimal medium containing kanamycin (10 μg/mL) to an optical density of 0.5 at 600 nm, induced with isopropyl-1-thio-β-D-galactopyranoside (0.5 mM), and grown for an additional 3 hr before harvesting. The cell pellet was suspended in buffer A (20 mM potassium phosphate [pH 7.0], 100 mM NaCl in 10% glycerol) and the protease inhibitor cocktail Complete-Mini EDTA-free (Roche Diagnostics) was added. Cells were lysed using an Emulsiflex homogenizer (Avestin, Inc., Canada), and debris was removed by centrifugation at 15,000 × g for 15 min. The supernatant was loaded on a Talon (Clonetech) column equilibrated with buffer A. The column was washed with buffer A containing 5 mM imidazole before eluting with buffer A containing 150 mM imidazole. Eluant from the Talon column was dialysed against buffer A, and the N-terminal $(His)_6$-tag was cleaved with thrombin (Novagen). The thrombin-cleaved protein was loaded on an SP-Sepharose column equilibrated in buffer A and was eluted with a gradient of 100–700 mM NaCl. Protein concentrations were determined using an extinction coefficient, ϵ_{280} = 64600 M^{-1} cm^{-1}, obtained by quantitative amino acid analysis.

Kinetic Analysis

Methylation assay and enzyme kinetics have been previously described in detail (Agarwalla et al., 2002). Briefly, enzymatic activity was measured by monitoring the transfer of radioactive methyl group from [^{3}H-Me]SAM to RNA. Reactions aliquots (20 μl) were adsorbed onto a DEAE paper, washed, and counted for tritium. For determinations of K_m and k_{cat} for the 37-mer substrate and the 12-mer substrate, the enzyme concentrations were 0.1 μM and 1 μM, respectively. RNA concentrations were varied from 1 to 40 μM. [^{3}H-Me]SAM concentration was 155 μM (1 Ci/0.3 mmol). The specific activities were measured using the RNA concentration of 10 μM and [^{3}H-Me]SAM concentration of 155 μM (1 Ci/0.3 mmol). For comparison of the wild-type and mutant enzymes, the 37-mer RNA (1932–1968, Dharmacon) was used as the substrate. Enzyme concentration was 0.1 μM for the wild-type and D363N mutant enzymes and 2 μM for the Q265E mutant enzyme. The detection limit of our assay at 2 μM enzyme concentration is ~2 mmole/min/mole, 1500-fold lower than the specific activity of the wild-type enzyme. For effects of the riboabasic modifications at positions 1937 and 1942, 37-mer wild-type substrate was compared with the 1937rab and 1942rab substrates. Enzyme concentration was 0.2 μM for the wild-type substrate, 1 μM for the A1937rab substrate, and 5 μM for the C1942rab substrate. To determine the k_{cat} and K_m for SAM, RNA concentration was 21 μM for the wild-type substrate and 44 μM the 1937rab substrate, and SAM concentrations were varied from 10 to 500 μM.

SDS-PAGE Analysis of Enzyme-Substrate Covalent Complexes

RumA (4 μM) and RNA (1932–1968, 4 μM) were mixed in a solution containing 100 mM Tris-HCl (pH 7.5), 1 mM $MgCl_2$, and 5 mM DTT in absence and presence of SAM (1 mM). The mixture was incubated at room temperature for 30 min before mixing with 2× SDS-PAGE loading buffer. The sample was applied to SDS-PAGE, and the gel was stained by Coomassie Blue after electrophoresis.

Supplemental Data

Supplemental Data include two figures and can be found with this article online at http://www.cell.com/cgi/content/full/120/5/599/DC1/.

Acknowledgments

We thank Janet Finer-Moore for help with structure determination and Pat Greene for critical reading of the manuscript. This work was supported by United States Public Health Service, National Institutes of Health Grant GM51232 (to R.M.S.).

Received: May 13, 2004
Revised: October 13, 2004
Accepted: December 23, 2004
Published: March 10, 2005

References

Agarwalla, S., Kealey, J.T., Santi, D.V., and Stroud, R.M. (2002). Characterization of the 23 S ribosomal RNA m^{5}U1939 methyltransferase from *Escherichia coli*. J. Biol. Chem. *277*, 8835–8840.

Agarwalla, S., Stroud, R.M., and Gaffney, B.J. (2004). Redox reac-

tions of the iron-sulfur cluster in a ribosomal RNA methyltransferase, RumA: optical and EPR studies. J. Biol. Chem. *279*, 34123–34129.

Anantharaman, V., Koonin, E.V., and Aravind, L. (2002). Comparative genomics and evolution of proteins involved in RNA metabolism. Nucleic Acids Res. *30*, 1427–1464.

Antson, A.A. (2000). Single-stranded-RNA binding proteins. Curr. Opin. Struct. Biol. *10*, 87–94.

Arcus, V. (2002). OB-fold domains: a snapshot of the evolution of sequence, structure and function. Curr. Opin. Struct. Biol. *12*, 794–801.

Ban, N., Nissen, P., Hansen, J., Moore, P.B., and Steitz, T.A. (2000). The complete atomic structure of the large ribosomal subunit at 2.4 Å resolution. Science *289*, 905–920.

Bashan, A., Agmon, I., Zarivach, R., Schluenzen, F., Harms, J., Berisio, R., Bartels, H., Franceschi, F., Auerbach, T., Hansen, H.A., et al. (2003). Structural basis of the ribosomal machinery for peptide bond formation, translocation, and nascent chain progression. Mol. Cell *11*, 91–102.

Brunger, A.T., Adams, P.D., Clore, G.M., Delano, W.L., Gros, P., Grosse-Kunstleve, R.W., Jiang, J.-S., Kuszewski, J., Nilges, N., Pannu, N.S., et al. (1998). Crystallography and NMR system (CNS): a new software system for macromolecular structure determination. Acta Crystallogr. D Biol. Crystallogr. *54*, 905–921.

Carson, M. (1997). Ribbons. In Methods of Enzymology, R.M. Sweet and C.W. Carter, eds. (New York: Academic Press), pp. 493–505.

Cheng, X., and Blumenthal, R.M. (2002). Cytosines do it, thymines do it, even pseudouridines do it—base flipping by an enzyme that acts on RNA. Structure (Camb.) *10*, 127–129.

CCP4 (Collaborative Computational Project, Number 4)(1994). The CCP4 suite: programs for protein crystallography. Acta Crystallogr. D Biol. Crystallogr. *50*, 760–763.

Decatur, W.A., and Fournier, M.J. (2002). rRNA modifications and ribosome function. Trends Biochem. Sci. *27*, 344–351.

Eiler, S., Dock-Bregeon, A., Moulinier, L., Thierry, J.C., and Moras, D. (1999). Synthesis of aspartyl-tRNA(Asp) in *Escherichia coli*—a snapshot of the second step. EMBO J. *18*, 6532–6541.

Fersht, A. (1999). Structure and Mechanism in Protein Science: A Guide to Enzyme Catalysis and Protein Folding (New York: W.H. Freeman and Company).

Freeland, S.J., Knight, R.D., and Landweber, L.F. (1999). Do proteins predate DNA? Science *286*, 690–692.

Fromme, J.C., and Verdine, G.L. (2003). Structure of a trapped endonuclease III-DNA covalent intermediate. EMBO J. *22*, 3461–3471.

Gu, X., and Santi, D.V. (1992). Covalent adducts between tRNA (m^5U54)-methyltransferase and RNA substrates. Biochemistry *31*, 10295–10302.

Hartley, B.S., and Kilby, B.A. (1954). The reaction of p-nitrophenyl esters with chymotrypsin and insulin. Biochem. J. *56*, 288–297.

Hoang, C., and Ferré-D'Amaré, A.R. (2001). Cocrystal structure of a tRNA Ψ55 pseudouridine synthase: nucleotide flipping by an RNA-modifying enzyme. Cell *107*, 929–939.

Hoffman, J.L. (1986). Chromatographic analysis of the chiral and covalent instability of *S*-adenosyl-L-methionine. Biochemistry *25*, 4444–4449.

Ishitani, R., Nureki, O., Nameki, N., Okada, N., Nishimura, S., and Yokoyama, S. (2003). Alternative tertiary structure of tRNA for recognition by a posttranscriptional modification enzyme. Cell *113*, 383–394.

Kabsch, W. (1976). A solution for the best rotation to relate two sets of vectors. Acta Crystallogr. A *32*, 922–923.

Kealey, J.T., Gu, X., and Santi, D.V. (1994). Enzymatic mechanism of tRNA (m^5U54)methyltransferase. Biochimie *76*, 1133–1142.

Klimasauskas, S., Kumar, S., Roberts, R.J., and Cheng, X. (1994). HhaI methyltransferase flips its target base out of the DNA helix. Cell *76*, 357–369.

Laskowski, R.A., MacArthur, M.W., Moss, D.S., and Thornton, J.M. (1993). PROCHECK: a program to check the stereochemical quality of protein structures. J. Appl. Crystallogr. *26*, 283–291.

Lee, T.T., Agarwalla, S., and Stroud, R.M. (2004). Crystal structure of RumA, an iron-sulfur cluster containing *E. coli* ribosomal RNA 5-methyluridine methyltransferase. Structure (Camb.) *12*, 397–407.

Lei, M., Podell, E.R., Baumann, P., and Cech, T.R. (2003). DNA self-recognition in the structure of Pot1 bound to telomeric single-stranded DNA. Nature *426*, 198–203.

Liu, L., and Santi, D.V. (1992). Mutation of asparagine 229 to aspartate in thymidylate synthase converts the enzyme to a deoxycytidylate methylase. Biochemistry *31*, 5100–5104.

Madsen, C.T., Mengel-Jorgensen, J., Kirpekar, F., and Douthwaite, S. (2003). Identifying the methyltransferases for m^5U747 and m^5U1939 in 23S rRNA using MALDI mass spectrometry. Nucleic Acids Res. *31*, 4738–4746.

Malone, T., Blumenthal, R.M., and Cheng, X. (1995). Structure-guided analysis reveals nine sequence motifs conserved among DNA amino-methyltransferases, and suggests a catalytic mechanism for these enzymes. J. Mol. Biol. *253*, 618–632.

Martinez Gimenez, J.A., Saez, G.T., and Seisdedos, R.T. (1998). On the function of modified nucleosides in the RNA world. J. Theor. Biol. *194*, 485–490.

Murshudov, G.N., Vagin, A.A., and Dodson, E.J. (1997). Refinement of macromolecular structures by the maximum-likelihood method. Acta Crystallogr. D Biol. Crystallogr. *53*, 240–255.

Murzin, A.G. (1993). OB(oligonucleotide/oligosaccharide binding)-fold: common structural and functional solution for non-homologous sequences. EMBO J. *12*, 861–867.

O'Gara, M., Klimasauskas, S., Roberts, R.J., and Cheng, X. (1996). Enzymatic C5-cytosine methylation of DNA: mechanistic implications of new crystal structures for H*ha*I methyltransferase-DNA-AdoHcy complexes. J. Mol. Biol. *261*, 634–645.

Otwinowski, Z., and Minor, W. (1997). Processing of X-ray diffraction data collected in oscillation mode. In Methods Enzymol., J.C.W. Carter and R.M. Sweet, eds. (New York: Academic Press), pp. 307–326.

Pan, H., Agarwalla, S., Moustakas, D.T., Finer-Moore, J., and Stroud, R.M. (2003). Structure of tRNA pseudouridine synthase TruB and its RNA complex: RNA recognition through a combination of rigid docking and induced fit. Proc. Natl. Acad. Sci. USA *100*, 12648–12653.

Perrakis, A., Morris, R., and Lamzin, V.S. (1999). Automated protein model building combined with iterative structure refinement. Nat. Struct. Biol. *6*, 458–463.

Perry, K.M., Fauman, E.B., Finer-Moore, J.S., Montfort, W.R., Maley, G.F., Maley, F., and Stroud, R.M. (1990). Plastic adaptation toward mutations in proteins: structural comparison of thymidylate synthases. Proteins *8*, 315–333.

Roberts, R.J., and Cheng, X. (1998). Base flipping. Annu. Rev. Biochem. *67*, 181–198.

Rozenski, J., Crain, P.F., and McCloskey, J.A. (1999). The RNA Modification Database: 1999 update. Nucleic Acids Res. *27*, 196–197.

Ruff, M., Krishnaswamy, S., Boeglin, M., Poterszman, A., Mitschler, A., Podjarny, A., Rees, B., Thierry, J.C., and Moras, D. (1991). Class II aminoacyl transfer RNA synthetases: crystal structure of yeast aspartyl-tRNA synthetase complexed with tRNA(Asp). Science *252*, 1682–1689.

Slupphaug, G., Mol, C.D., Kavli, B., Arvai, A.S., Krokan, H.E., and Tainer, J.A. (1996). A nucleotide-flipping mechanism from the structure of human uracil-DNA glycosylase bound to DNA. Nature *384*, 87–92.

Solie, T.N., and Schellman, J.A. (1968). The interaction of nucleosides in aqueous solution. J. Mol. Biol. *33*, 61–77.

Suck, D. (1997). Common fold, common function, common origin? Nat. Struct. Biol. *4*, 161–165.

Valle, M., Gillet, R., Kaur, S., Henne, A., Ramakrishnan, V., and Frank, J. (2003). Visualizing tmRNA entry into a stalled ribosome. Science *300*, 127–130.

Winn, M.D., Isupov, M.N., and Murshudov, G.N. (2001). Use of TLS

parameters to model anisotropic displacements in macromolecular refinement. Acta Crystallogr. D Biol. Crystallogr. *57*, 122–133.

Wu, J.C., and Santi, D.V. (1985). On the mechanism and inhibition of DNA cytosine methyltransferases. Prog. Clin. Biol. Res. *198*, 119–129.

Xiong, Y., and Steitz, T.A. (2004). Mechanism of transfer RNA maturation by CCA-adding enzyme without using an oligonucleotide template. Nature *430*, 640–645.

Yusupov, M.M., Yusupova, G.Z., Baucom, A., Lieberman, K., Earnest, T.N., Cate, J.H., and Noller, H.F. (2001). Crystal structure of the ribosome at 5.5 Å resolution. Science *292*, 883–896.

Accession Numbers

The coordinates of the RumA-RNA-SAH complex have been deposited in the Protein Data Bank under the accession code 2BH2.